J|A|C|S ARTICLES

Published on Web 06/11/2010

Iridium Compounds with κ-*P,P,Si* (biPSi) Pincer Ligands: Favoring Reactive Structures in Unsaturated Complexes

Eduardo Sola,* Alba García-Camprubí, José L. Andrés, Marta Martín, and Pablo Plou

Departamento de Química de Coordinación y Catálisis Homogénea, Instituto de Ciencia de Materiales de Aragón, CSIC-Universidad de Zaragoza, E-50009 Zaragoza, Spain

Received March 24, 2010; E-mail: sola@unizar.es

Abstract: The structure, coordination properties, insertion processes, and dynamic behavior in solution of the five-coordinate complexes [IrXH(biPSi)] (biPSi = κ-*P,P,Si*-Si(Me){$(CH_2)_3PPh_2$}$_2$; X = Cl (**1**), Br (**2**), or I (**3**)) have been investigated. The compounds are formed as mixtures of two isomers, *anti* and *syn*, in slow equilibrium in solution. The equilibrium position depends on the halogen and the solvent. Both isomers display distorted square-based pyramidal structures in which the vacant position sits *trans* to silicon. The equatorial plane of the *syn* isomer is closer to the T structure due to distortions of steric origin. The small structural differences between the isomers trigger remarkable differences in reactivity. The *syn* isomers form six-coordinate adducts with chlorinated solvents, CO, $P(OMe)_3$, or NCMe, always after ligand coordination *trans* to silicon. The *anti* isomers do not form detectable adducts with chlorinated solvents and coordinate CO or $P(OMe)_3$ either *trans* to silicon (kinetic) or *trans* to hydride (thermodynamic). NCMe coordinates the *anti* isomers exclusively at the position *trans* to hydride. Qualitative and quantitative details (equilibrium constants, enthalpies, entropies, etc.) on these coordination processes are given and discussed. As a result of the different coordination properties, insertion reagents such as acetylene, diphenylacetylene, or the alkylidene resulting from the decomposition of ethyl diazoacetate selectively insert into the Ir−H bond of **1**-*syn*, not into that of **1**-*anti*. These reactions give five-coordinate *syn* alkenyl or alkyl compounds in which the vacancy also sits *trans* to silicon. Acetylene is polymerized in the coordination sphere of **1**. The nonreactive isomer **1**-*anti* also evolves into the *syn* insertion products via *anti*↔*syn* isomerizations, the rates of which are notably dependent on the nature of the insertion reactants. H_2 renders *anti*↔*syn* isomerization rates of the same order as the NMR time scale. The reactions are second order (k_{obs} = k(*anti*↔*syn*)[H_2]) and do not involve H_2/IrH hydrogen atom scrambling. A possible isomerization mechanism, supported by MP2 calculations and compatible with the various experimental observations, is described. It involves Ir(V) intermediates and a key σ Ir-(η^2-SiH) agostic transition state. A similar transition state could also explain the *anti*↔*syn* isomerizations in the absence of oxidative addition reactants, although at the expense of high kinetic barriers strongly dependent on the presence of potential ligands and their nature.

Introduction

Coordinatively unsaturated transition metal complexes are ubiquitous in catalytic transformations as either catalyst precursors or reaction intermediates, or both.[1] Depending on the catalytic application, these complexes coordinate "reactive" ligands such as hydride, alkyl, alkenyl, acyl, carbene, etc.—all of them strong σ-donors and therefore good *trans*-directors.[2] Accordingly, these ligands push coordination vacancies *trans* to them,[3] thus favoring structures which are generally inappropriate for catalytic applications following ordinary inner-sphere mechanisms. As a consequence, the catalytic cycles must include reorganization steps through which the catalysts make available to the incoming substrates vacancies *cis* to the reactive ligands. Such reorganizations—typically distortions, isomerizations, or further ligand dissociations—require additional energetic contributions that may prejudice kinetics, although, especially in cases of ligand dissociation, the negative effects can go even further and jeopardize catalyst stability. A good example of this can be found in Grubbs' catalyst [$RuCl_2$(=CHPh)$(PCy_3)_2$],[4] a d^6 square-pyramidal compound with the vacancy *trans* to the carbene ligand. Despite its coordinative unsaturation, this complex starts catalysis only after phosphine dissociation to form a 14 e^- species; this process is responsible for practical difficulties such as the need for an initiation period, the limited catalyst life, and the incompatibility of this catalyst with others in tandem processes.[5] Subsequent generations of olefin metathesis catalysts derived from this compound have minimized the extent of such drawbacks,[6] although they retain the adverse structure that is their origin.

(1) Van Leeuwen, P. W. N. M. *Homogeneous Catalysis. Understanding the Art*; Kluwer Academic Publishers: Dordrecht, 2004.
(2) Coe, B. J.; Glenwright, S. J. *Coord. Chem. Rev.* **2000**, *203*, 5–80.
(3) Jean, Y. *Molecular Orbitals of Transition Metal Complexes*; Oxford University Press: New York, 2005.
(4) Grubbs, R. H. *Tetrahedron* **2004**, *60*, 7117–7140.
(5) Goldman, A. S.; Roy, A. H.; Huang, Z.; Ahuja, R.; Schinski, W.; Brookhart, M. *Science* **2006**, *312*, 257–261.
(6) *Handbook of Metathesis*; Grubbs, R. H., Ed.; Wiley-VCH: Weinheim, 2003.

The adoption of such unfavorable structures can be combated through ligand design. An obvious strategy toward this end is to use polydentate rigid ligands such as the *fac*-coordinating Cp and Tp,[7] much of whose success in catalysis might be attributed to their ability to confine reactive ligands and coordination vacancies mutually *cis*.[8] A second alternative, a priori compatible with different ligand types and coordination modes, would be based on ancillary ligands more *trans*-directing than those referred to above as reactive. Following generally accepted conclusions on this subject,[2,9] this would only be within the reach of anionic ligands such as carbine, sulfide, oxide, nitride, bent nitrosyl, stannyl, silyl, or boryl. Among them, stannyl,[10] silyl,[11] and boryl[12] ligands could indeed engender a variety of stereoelectronic environments attractive for catalysis, although, due to their high reactivity, a stabilization rendering them *ancillary* would be necessary. This has already been found feasible for silyl moieties within polydentate ligands of the types *κ-P,P,Si* (biPSi)[13,14] and *κ-N,N,Si*[15] which, in addition, have emerged capable of stabilizing coordinatively unsaturated compounds and catalysts.[16]

The above considerations suggest that this type of silyl-containing ligands is likely to confer kinetic advantages to their complexes and drive genuine reactivities and catalytic properties. In order to substantiate these potential pros and characterize possible cons, we have conducted this study on the five-coordinate d^6 complexes [IrXH(biPSi)] (X = halogenide; biPSi = *κ-P,P,Si*-Si(Me){$(CH_2)_3PPh_2$}$_2$) focusing on basic aspects of their chemistry that are likely affected by the peculiar characteristics of the biPSi pincer ligand:[17] structure, coordination properties, and dynamic behavior in solution. The study confirms that the silyl entity can indeed induce distinctive, more reactive, ground-state structures in five-coordinate hydride, alkenyl, and alkyl iridium(III) complexes but also concludes other less-anticipated features. Thus, the severe weakening of the bonds *trans* to silicon intensifies the relative impact of steric factors over coordination, enabling effective discriminations from otherwise negligible differences. Also worth mentioning is the accessibility of agostic Ir-(η^2-SiH) transition states (TSs), a genuine reactivity resource that widens and simplifies the chemistry of hydride derivatives.

Results and Discussion

Isomers of [IrXH(biPSi)] and Structures. The complex [IrClH(biPSi)] (**1**) was previously reported to result from the reaction between dimer [Ir(μ-Cl)(cod)]$_2$ and the biPSi ligand precursor HSi(Me){$(CH_2)_3PPh_2$}$_2$.[13] On the basis of the NMR data obtained from freshly prepared solutions in $CDCl_3$, **1** was described as a single isomer displaying an *anti* orientation of the hydride ligand relative to the methyl group at silicon (**1**-*anti*, eq 1). Nevertheless, we have now observed that, after several days at room temperature, these solutions evolve equilibrium mixtures of the two isomers, **1**-*anti* and **1**-*syn*. The position of the **1**-*anti*:**1**-*syn* equilibrium is 93:7 in C_6D_6 or toluene-d_8, irrespective of the temperature, but slightly diminishes to ca. 83:17 in solvents such as $CDCl_3$ or CD_2Cl_2. The ^{1}H NOESY NMR spectra of these mixtures display clear cross-peaks between the hydride and methyl signals of the minor isomer, thus confirming the relative *syn* orientation of these groups (eq 1).

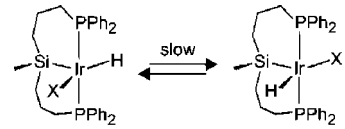

1-3-*anti* **1-3**-*syn* (1)

X = Cl(**1**), Br(**2**), I(**3**)

Analogues of **1** with bromide and iodide ligands instead of chloride have been obtained by reaction of CH_2Cl_2 solutions of **1** with the corresponding sodium halogenide in excess. The compounds [IrBrH(biPSi)] (**2**) and [IrIH(biPSi)] (**3**) have also been isolated as kinetic mixtures of *anti* and *syn* isomers, the compositions of which depend on the actual reaction conditions and isolation procedures. As for **1**, these kinetic mixtures have been observed to slowly evolve solvent-dependent *anti*:*syn* equilibria. The bromide complex **2** behaves similarly to its chloride precursor, affording *anti*:*syn* equilibria of molar compositions 92:8 and 82:18 in C_6D_6 and $CDCl_3$, respectively. The equilibrium proportion of the *syn* isomer is larger for the iodide compound **3**, which gives rise to nearly equimolar mixtures in C_6D_6, 45:55, but enriched in the *syn* isomer in CD_2Cl_2 or $CDCl_3$, ca. 22:78.

The X-ray structures of the two isomeric bromide complexes, **2**-*anti* and **2**-*syn*, are shown in Figure 1. Relevant bond distances and angles of these two structures, together with those of **3**-*syn*, can be found as Supporting Information. Both isomers **2** display distorted square-based pyramidal structures in which the vacant position sits *trans* to silicon. This is in contrast with the structures adopted by isoelectronic analogues of **2** coordinating other pincer diphosphines with sp^2 carbon or nitrogen donor atoms, in which the vacant site is *trans* to hydride.[18] Then the structures confirm that, as expected, the *trans* influence of the sp^3 silicon dominates over that of hydride, rendering isoelectronic five-coordinate d^6 complexes non-isostructural.

The small structural differences between isomers **2** deserve careful consideration since, as will be described below, they

(7) Trofimenko, S. *Scorpionates. The Coordination Chemistry of Polypyrazolylborate Ligands*; Imperial College Press: London, 1999.
(8) Best examples are in olefin polymerizations catalyzed by group 4 metalocenes. See: Resconi, L.; Chadwick, J. C.; Cavallo, L. In *Comprehensive Organometallic Chemistry*, 3rd ed.; Mingos, D. M. P., Crabtree, R. H., Eds.; Elsevier: Amsterdam, 2006; Vol. 4, pp 1006−1166.
(9) Zhu, J.; Lin, Z.; Marder, T. B. *Inorg. Chem.* **2005**, *44*, 9384–9390.
(10) Smith, N. D.; Mancuso, J.; Lautens, M. *Chem. Rev.* **2000**, *100*, 3257–3282.
(11) Corey, J. Y.; Braddock-Wilking, J. *Chem. Rev.* **1999**, *99*, 175–292.
(12) Irvine, G. J.; Lesley, M. J. G.; Marder, T. B.; Norman, N. C.; Rice, C. R.; Robins, E. G.; Roper, W. R.; Whittell, G. R.; Wright, L. J. *Chem. Rev.* **1998**, *98*, 2685–2722.
(13) Stobart, S. R.; Brost, R. D.; Bruce, G. C.; Joslin, F. L. *Organometallics* **1997**, *16*, 5669–5680.
(14) (a) Bushnell, G. W.; Casado, M. A.; Stobart, S. R. *Organometallics* **2001**, *20*, 601–603. (b) Auburn, M. J.; Holmes-Smith, R. D.; Stobart, S. R.; Bakshi, P. K.; Cameron, T. S. *Organometallics* **1996**, *15*, 3032–3036. (c) Grundy, S. L.; Holmes-Smith, R. D.; Stobart, S. R.; Williams, M. A. *Inorg. Chem.* **1991**, *30*, 3333–3337. (d) MacInnis, M. C.; MacLean, D. F.; Lundgren, R. J.; McDonald, R.; Turculet, L. *Organometallics* **2007**, *26*, 6522–6525. (e) MacLean, D. F.; McDonald, R.; Ferguson, M. J.; Caddell, A. J.; Turculet, L. *Chem. Commun.* **2008**, 5146–5148. (f) Morgan, E.; MacLean, D. F.; McDonald, R.; Turculet, L. *J. Am. Chem. Soc.* **2009**, *131*, 14234–14236.
(15) (a) Sangtrirutnugul, P.; Tilley, T. D. *Organometallics* **2007**, *26*, 5557–5568. (b) Sangtrirutnugul, P.; Tilley, T. D. *Organometallics* **2008**, *27*, 2223–2230. (c) Sangtrirutnugul, P.; Stradiotto, M.; Tilley, T. D. *Organometallics* **2006**, *25*, 1607–1617. (d) Stradiotto, M.; Fujdala, K. L.; Tilley, T. D. *Chem. Commun.* **2001**, 1200–1201.
(16) This capability has also been recognized for boryl moieties in pincer phosphines: (a) Segawa, Y.; Yamashita, M.; Nozaki, K. *J. Am. Chem. Soc.* **2009**, *131*, 9201–9203. (b) Segawa, Y.; Yamashita, M.; Nozaki, K. *Organometallics* **2009**, *28*, 6234–6242.
(17) (a) *The Chemistry of Pincer Compounds*; Morales-Morales, D., Jensen, C., Eds.; Elsevier: Amsterdam, 2007. (b) van der Boom, M. E.; Milstein, D. *Chem. Rev.* **2003**, *103*, 1759–1792. (c) Albrecht, M.; van Koten, G. *Angew. Chem., Int. Ed.* **2001**, *41*, 3750–3781.

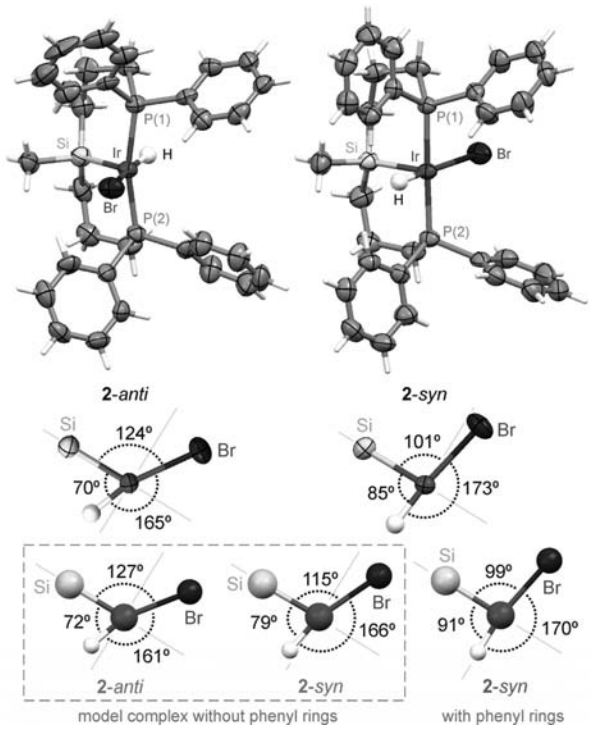

Figure 1. (Top) X-ray structures of isomers **2** and angles of their equatorial planes. (Bottom) Equatorial planes of MP2-optimized models of isomers **2** without and with phenyl rings.

trigger remarkable differences in reactivity. The geometry of the *syn* isomer displays little deviation from an octahedron with a vacant position, showing bond angles around the metal close to 90 and 180° (T structure).[3] On the other hand, the P−Ir−P angle of the *anti* isomer decreases to 163°, while the distribution of ligands in the equatorial plane approaches that of a distorted trigonal bipyramid (Y structure). Since these differences are likely to result from steric and conformational adjustments within a common electronically preferred structure,[19] we have optimized the geometries of various models for isomers **2** to understand the structural impact of each separate contribution. The MP2-based optimization of model complexes without phenyl rings (H instead of Ph) reproduces the experimental disposition of equatorial ligands only for the most stable isomer **2**-*anti*, suggesting that repulsions coming from the axial substituents do not contribute to this structure (Figure 1, bottom). This is despite the fact that such steric contributions are usually important in the presence of pincer-type diphophines, for which the ligand skeleton imposes an eclipsed conformation of the two PR_2 moieties that maximizes their steric impact on the equatorial plane.[20] In agreement with this latter observation, the model of isomer **2**-*syn* indeed requires the inclusion of phenyls

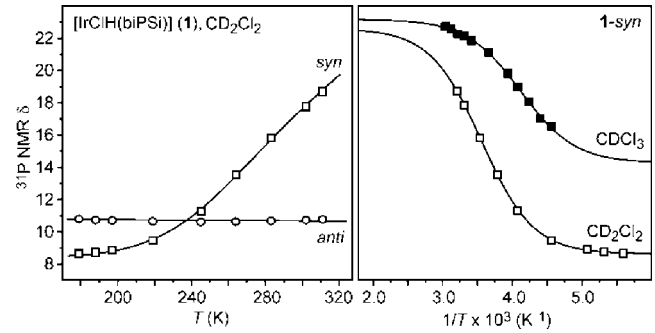

Figure 2. (Left) Variation with temperature of the ^{31}P NMR chemical shifts of isomers **1** in CD_2Cl_2. (Right) Sigmoidal plots on the ^{31}P NMR chemical shift dependence upon $1/T$ for **1**-*syn*.

(UFF methods in ONIOM approach) to afford an optimized structure close to the experimental one.

Thus, contrary to what the geometric regularity of isomer **2**-*syn* seems to suggest, the structure of **2**-*anti* is the electronically preferred one, whereas that of **2**-*syn* results from distortions provoked by the sterics. Examination of space-filling models indicates that the bromide ligand of **2**-*anti* occupies a position very conflicting in steric terms, wedged among four phenyl rings regardless of its exact position in the equatorial plane. Since there is no way to avoid or minimize such steric conflict, there is no reason to distort. In contrast, the halide of the *syn* isomer can elude any conflict with the phenyls by approaching the silyl moiety. Hence, there is a privileged halide position from the steric point of view and, consequently, a good reason to distort. According to the available structural data, the characteristic structure of each isomer is retained by changing the halogenide. In contrast, the relative energies of the isomers are likely to vary with halogen size, progressively disfavoring the more encumbered *anti* isomers. This qualitative observation explains the relative destabilization of the iodide complex **3**-*anti* observed experimentally.

Coordination Properties. As a result of their subtle structural differences, the *syn* and *anti* isomers of [IrXH(biPSi)] complexes constitute slightly different starting points for the formation of six-coordinate adducts. Coordination *trans* to silicon should be relatively favored in the distorted *syn* isomers, which are preorganized to form octahedral compounds. This advantage can be readily recognized by the potential ligands, especially by those weakly coordinating. Figure 2 illustrates the temperature dependence of the ^{31}P NMR chemical shifts corresponding to the *anti* and *syn* isomers of **1** in CD_2Cl_2, which can be interpreted as the result of a solvent coordination equilibrium exclusively affecting to the *syn* isomer (eq 2).[21] The phenomenon has also been observed, by ^1H and ^{31}P NMR, for the *syn* isomers of the analogous complexes **2** and **3** in both $CDCl_3$ and CD_2Cl_2. The dependences of ^{31}P NMR chemical shifts on the inverse of temperature have been adjusted to symmetric sigmoidal functions (Figure 2, right) to directly estimate the $\Delta H°$ and $\Delta S°$ thermodynamic parameters of the proposed solvent coordination. Values of $\Delta H°$ in the range $-5.5(\pm0.5)$ kcal mol^{-1} and negative enthalpy increments $\Delta S°$ of about $-26(\pm2)$ cal K^{-1} mol^{-1} have been obtained, irrespective of the compound and the solvent (see Experimental Section and Supporting Information for details). This small additional

(18) Representative structures: (a) Göttker-Schnetmann, I.; White, P.; Brookhart, M. *J. Am. Chem. Soc.* **2004**, *126*, 1804–1811. (b) Grimm, J. C.; Nachtigal, C.; Mack, H.-G.; Kaska, W. C.; Mayer, H. A. *Inorg. Chem. Commun.* **2000**, *3*, 511–514. (c) Ben-Ari, E.; Gandelman, M.; Rozenberg, H.; Shimon, L. J. W.; Milstein, D. *J. Am. Chem. Soc.* **2003**, *125*, 4714–4715.

(19) Other possible causes of distortion such as the formation of agostic or hypervalent interactions can be discarded in the view of the distances around the Si atoms. See: Nikonov, G. I. *Adv. Organomet. Chem.* **2005**, *53*, 217–309.

(20) (a) Gusev, D. G.; Lough, A. J. *Organometallics* **2002**, *21*, 5091–5099. (b) Ujaque, G.; Maseras, F.; Eisenstein, O.; Liable-Sands, L.; Rheingold, A. L.; Yao, W.; Crabtree, R. H. *New J. Chem.* **1998**, 1493–1498.

(21) Precedents for CH_2Cl_2 coordination to Ir(III): (a) Klei, S. R.; Golden, J. T.; Burger, P.; Bergman, R. G. *J. Mol. Catal. A* **2002**, *189*, 79–94. (b) Arndtsen, B. A.; Bergman, R. G. *Science* **1995**, *270*, 1970–1973.

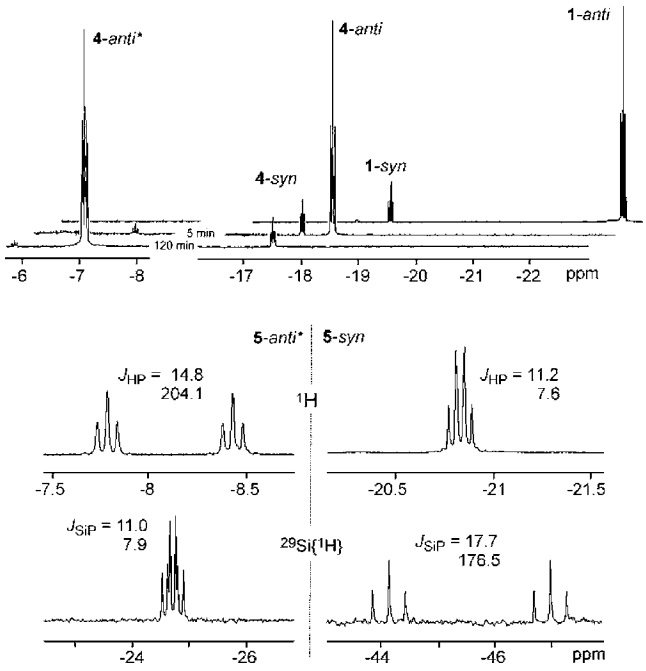

Figure 3. (Top) Hydride ^{1}H NMR signals of **1** (upper spectrum) and its kinetic and thermodynamic products of reaction with CO, respectively (C_6D_6, 300 K). (Bottom) Hydride ^{1}H and ^{29}Si{^{1}H} NMR signals of isomers **5**-*anti** (left) and **5**-*syn* (right) in $CDCl_3$.

stabilization of the *syn* isomers accounts for the aforementioned dependence of the *anti*:*syn* equilibrium position upon the solvent.

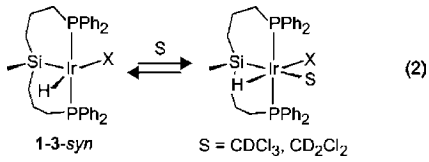

(2)

A more complete picture on the coordination capabilities of the [IrXH(biPSi)] complexes has been obtained from their reactions with the small and strongly coordinating CO. Figure 3 illustrates how both isomers of **1** initially coordinate CO at the position *trans* to silicon to form the [IrClH(biPSi)(CO)] adducts, **4**-*anti* and **4**-*syn*. The kinetic product **4**-*anti* then further evolves into a new compound which, attending to its NMR parameters, is another *anti* isomer (NOE) and coordinates CO at the position *trans* to hydride. The latter is inferred from the marked displacement of the ^{1}H NMR signal corresponding to the hydride, from δ −19.97 to −7.05, consistent with the coordination of a π-acceptor ligand *trans* to it.[22] The structure of this new coordination isomer, referred to as *anti**, can be unambiguously assigned with the help of adduct [IrClH(biPSi){P(OMe)$_3$}] (**5**), the P(OMe)$_3$ analogue of **4**. This compound has also been observed to initially form a kinetic mixture of isomers **5**-*anti* and **5**-*syn*, subsequently evolving into an equilibrium of **5**-*anti** and **5**-*syn*. Figure 3 shows the characteristic J_{HP} and J_{SiP} NMR coupling constants that confirm the structures proposed in eq 3.

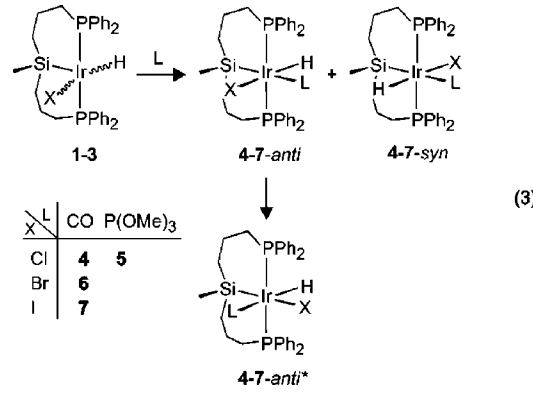

(3)

The *anti**:*syn* equilibrium distributions found for the CO and P(OMe)$_3$ adducts **4** and **5** (98:2 and 85:15, respectively) are rather similar despite the different ligand size. In contrast, changing the halogenide ligand has a very large effect on the composition of the *anti**:*syn* equilibrium, which shifts to 48:52 for the bromide adduct [IrBrH(biPSi)(CO)] (**6**) and to 0:100 for the iodide analogue **7**. Thus, looking exclusively at the thermodynamic distributions of isomers (those observable after several hours under CO), the simple replacement of chloride by iodide inverts the stereochemistry of the reaction product and switches the CO coordination position from *trans* to hydride (98%) to *trans* to silicon (100%). Even though this result can be rationalized on the basis of conventional steric arguments already pointed out in the previous section, its forcefulness exceeds the commonly modest nature of the halide effects.[23]

In the same line of extreme behaviors, a ligand such as acetonitrile has been found to bind each isomer of complexes **1**−**3** at a different site. At room temperature and in the presence of a moderate acetonitrile excess, the ^{1}H NMR spectra of solutions of **1**−**3** in $CDCl_3$ or toluene-d_8 have been observed to display narrow signals corresponding to the *syn* adducts [IrXH(biPSi)(NCMe)] {X = Cl (**8**), Br (**9**), and I (**10**)} but broad ones attributable to *anti* isomers (Figure 4). Decoalescence of the latter signals at low temperature has evidenced slow equilibria between the five-coordinate *anti* precursors and their acetonitrile adducts. Integration of the corresponding ^{1}H hydride and acetonitrile signals in the low-temperature NMR spectra has afforded the equilibrium constants at each temperature. In addition, these spectra have allowed identification of the coordination position for acetonitrile, which is that *trans* to hydride (*anti**). This follows from the ^{13}C signals corresponding to the quaternary carbon of the acetonitrile ligand (N*C*Me) with and without decoupling of the hydride ^{1}H resonance (Figure 4), which evidence a $^3J_{CH}$ coupling constant of 9.8 Hz only compatible with a *trans* relative position of hydride and NCMe. On the other hand, the NMR signals corresponding to the *syn*

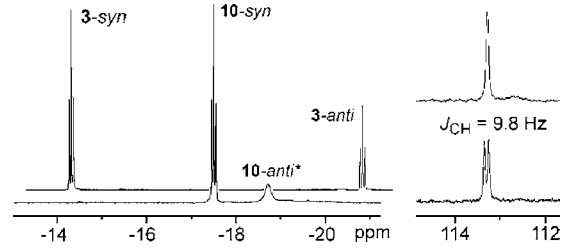

Figure 4. (Left) Room-temperature hydride ^{1}H NMR signals of **3** in $CDCl_3$, before and after addition of 10 equiv of acetonitrile. (Right) ^{13}C NMR signal corresponding to the N*C*Me ligand of **8**-*anti** at 223 K: (top) ^{13}C{^{1}H} and (bottom) allowing hydride coupling.

(22) For examples, see: (a) Sola, E.; Navarro, J.; López, J. A.; Lahoz, F. J.; Oro, L. A.; Werner, H. *Organometallics* **1999**, *18*, 3534–3546. (b) Navarro, J.; Sola, E.; Martín, M.; Dobrinovitch, I. T.; Lahoz, F. J.; Oro, L. A. *Organometallics* **2004**, *23*, 1908–1917. (c) Sola, E.; Bakhmutov, V. I.; Torres, F.; Elduque, A.; López, J. A.; Lahoz, F. J.; Werner, H.; Oro, L. A. *Organometallics* **1998**, *17*, 683–696.

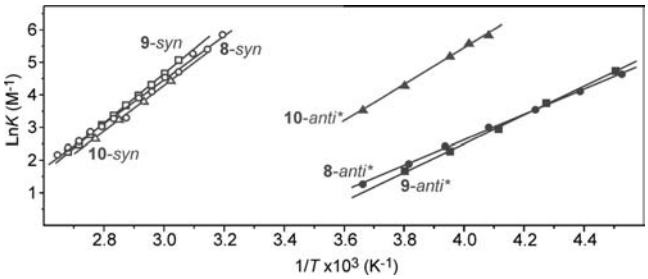

Figure 5. Van't Hoff representation of the equilibrium constants for acetonitrile coordination to **1**−**3** to form **8**−**10**, experimentally determined by NMR in toluene-d_8.

Table 1. Enthalpies and Entropies of Formation of the Acetonitrile Adducts **8**−**10**

X	isomer	$\Delta H°$ (kcal mol^{-1})	$\Delta S°$ (cal K^{-1} mol^{-1})
Cl	**8**-*anti**	−7.7(±0.4)	−26(±2)
Cl	**8**-*syn*	−13.4(±0.6)	−31(±2)
Br	**9**-*anti**	−8.7(±0.5)	−30(±2)
Br	**9**-*syn*	−15.1(±0.9)	−36(±2)
I	**10**-*anti**	−11.2(±0.7)	−34(±3)
I	**10**-*syn*	−13.9(±1.3)	−33(±3)

isomers of **8**−**10** reveal the coordination equilibria of eq 4 only above 300 K, when the equilibrium concentrations of the five-coordinate precursors **1**−**3**-*syn* become significant. Under such conditions, the equilibria are fast on the NMR time scale and, as detailed above for the coordination of chlorinated solvents, generate averaged signals whose temperature-dependent chemical shifts permit quantitative determinations of the equilibrium positions.

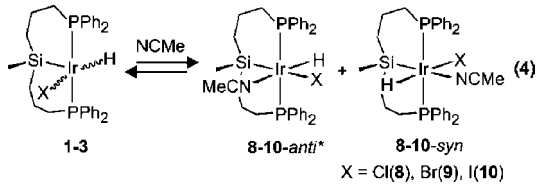

Before discussing the quantitative aspects of acetonitrile coordination to **1**−**3**, it should be noted that, irrespective of the compound and the isomer, the equilibria in eq 4 are established much faster (seconds) than those converting *anti* species into *syn* and vice versa (days). Hence, each five-coordinate isomer can be assumed to be in equilibrium with its corresponding acetonitrile adduct even if the *anti*:*syn* composition, which evolves very slowly, is outside equilibrium. In fact, the equilibria of eq 4 have been quantified by NMR despite the isomers **8**−**10**-*anti** eventually disappearing in favor of their more stable *syn* isomers. The Van't Hoff representations (ln K vs $1/T$) of the experimentally determined equilibrium constants are shown in Figure 5, and the adduct formation enthalpies and entropies estimated from these representations are listed in Table 1.

According to these experimental determinations, the three *syn* acetonitrile adducts display indistinguishable thermodynamic properties, including a common formation enthalpy of about 14 kcal mol^{-1} and negative entropy increments around −33 cal K^{-1} mol^{-1}. The *anti** adducts are less stable than their *syn* isomers, in agreement with their eventual disappearance from the product mixtures. The chloride and bromide complexes **8**- and **9**-*anti** show equal thermodynamic values, but the equilibrium constants of the iodide analogue **10**-*anti** are about 1 order of magnitude higher and lead to a higher formation enthalpy. Rather than a greater stability of this iodide adduct, the improved thermodynamic balance likely reflects, once again, the lower stability of the precursor **3**-*anti*. Besides steric factors, the smaller π-donating capability of iodide compared to that of chloride and bromide could be added to the list of possible causes for the different thermodynamics,[23] since such a bond contribution must disappear in the six-coordinated adducts.

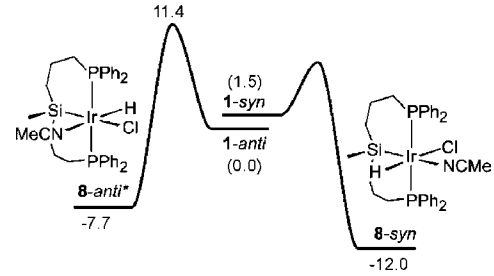

Figure 6. Experimental enthalpy profile for the coordination of acetonitrile to **1** in toluene. The 1.5 kcal mol^{-1} difference between isomers **1** follows from the *anti*:*syn* equilibrium position in toluene (93:7), considering $\Delta S° = 0$.

First-order rate constants for acetonitrile dissociation (k_{-1}) have been measured for complex **8**-*anti** in toluene-d_8 between 273 and 236 K. Within this temperature range, the hydride ^{1}H NMR signals of both complexes in equilibrium were simultaneously observable, while the rate constants remained of a magnitude accessible by spin saturation transfer methods. These rate constants have allowed an estimation of the activation parameters for acetonitrile dissociation from **8**-*anti** as $\Delta H^{\ddagger} =$ 19.1(±0.7) kcal mol^{-1} and $\Delta S^{\ddagger} = 20(\pm 2)$ cal K^{-1} mol^{-1}. Unfortunately, a similar quantitative determination has not been possible for the **8**-*syn* isomer, although its narrow ^{1}H NMR averaged acetonitrile resonance (free + coordinated to **8**-*syn*) at 236 K ensures that the equilibrium between *syn* species remains fast on the NMR time scale. Assuming similar activation entropies for ligand dissociation from both isomers **8**, this acetonitrile resonance line width would imply a dissociation enthalpy from **8**-*syn* significantly below that estimated for **8**-*anti**. This latter qualitative consideration, together with the quantitative data collected for **8**, are used to assemble the energy profile of Figure 6, which summarizes the experimental observations on acetonitrile coordination to complex **1**. The figure highlights the different coordination position of acetonitrile in each isomer and the fact that the *syn* adduct is simultaneously more stable and more labile than its *anti** isomer.

Figure 7 shows the X-ray structures of two *syn* adducts already described in this section, **6**-*syn* and **8**-*syn*. At this point of the discussion, their perfectly octahedral structures deserve no comment except for their long Ir−C and Ir−N distances *trans* to silicon, 1.958(3) and 2.148(5) Å, respectively (see Supporting Information for more structural details). The latter is similar to the bond lengths of other labile acetonitrile ligands *trans* to hydrides or alkenyls in related Ir(III) compounds.[22,24] Although we have not been able to grow suitable crystals for any of the *anti* or *anti** isomers in this section, Figure 7 includes the

(23) Fagnou, K.; Lautens, M. *Angew. Chem., Int. Ed.* **2002**, *41*, 26–47.

(24) (a) Martín, M.; Torres, O.; Oñate, E.; Sola, E.; Oro, L. A. *J. Am. Chem. Soc.* **2005**, *127*, 18074–18084. (b) Canepa, G.; Sola, E.; Martín, M.; Lahoz, F. J.; Oro, L. A.; Werner, H. *Organometallics* **2003**, *22*, 2151–2160.

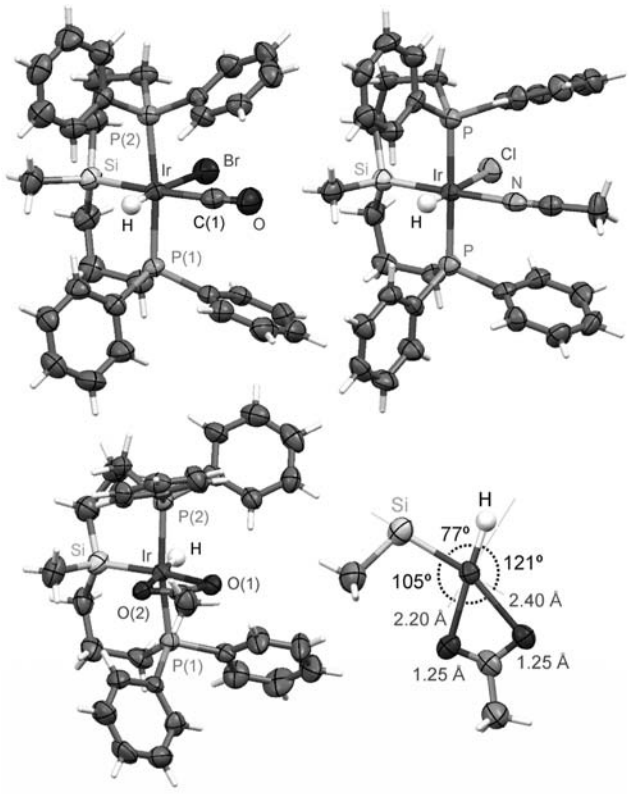

Figure 7. X-ray structures of **6**-*syn*, **8**-*syn*, and **11**-*anti* and detail of the **11**-*anti* equatorial plane.

illustrative structure of the complex *anti*-[Ir(O_2CMe)H(biPSi)] (**11**-*anti*). This compound has been prepared from **1** and sodium acetate in an analogous manner to **2** and **3**, and its *anti*:*syn* equilibrium contains 95% of the *anti* isomer. From the perspective of the acetate ligand, this compound is six-coordinate since, as inferred from the two equal C−O distances, 1.253(6) and 1.255(6) Å, the coordination mode of acetate is chelate (κ^2-*O*). However, attending to the iridium coordination sphere, the complex is best described as five-coordinate, since the Ir−O distance *trans* to silicon, 2.405(4) Å, is too long for a bond.[25] The example illustrates how, even under almost optimal conditions, the *anti* fragments hardly show the Lewis acidity that can be expected from its coordinative unsaturation.

Insertions. Not surprisingly, given the coordination behavior described in the previous section, an insertion reagent such as diphenylacetylene has been found to selectively react with the *syn* isomer of complex **1**, leaving unreacted **1**-*anti*. The new reaction product is the five-coordinate alkenyl complex *syn*-[IrCl{*Z*-C(Ph)═CHPh}(biPSi)] (**12**) (eq 5), as indicated by the clear ^{1}H NOESY NMR cross peaks relating the vinylic hydrogen signal with that corresponding to the methyl substituent at silicon. Monitoring the reaction by NMR at room temperature for weeks (or days at high temperature in toluene-d_8) has revealed the eventual quantitative formation of **12** as a consequence of the slow equilibration between the *anti* and *syn* isomers of precursor **1**. Actually, this evolution has been used to estimate the rate constant for the *anti*↔*syn* isomerization process, assumed to be rate-limiting in the reaction sequence leading to **12**. The kinetic information will be discussed in the next section.

(25) Examples of this long distance are restricted to water and hydroxide ligands formally acting as asymmetric bridges between metals. See: Allen, F. H. *Acta Crystallogr.* **2002**, *B58*, 380–388.

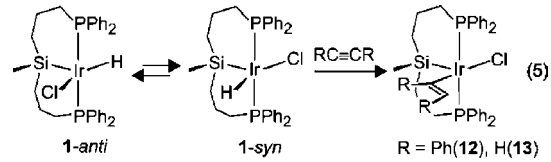

Many features of the insertion reaction in eq 5 change substantially by changing the alkyne from diphenylacetylene (bulky and internal) to acetylene (small and terminal). Actually, the only similarity between the two reactions has been the isolation of analogous *syn* insertion products—the vinyl complex *syn*-[IrCl(CH═CH_2)(biPSi)] (**13**) in the case of acetylene. In connection with the main issue this work addresses, the T structure of **13** shown in Figure 8 confirms that the sp^3 silicon donor atom is able to place the coordination vacancy in the *trans* position also in the presence of an alkenyl, another *trans*-directing ligand assiduous in many catalytic transformations. For comparison, the structure of complex [IrCl(CH═CHPh)(PCP)], an analogue of **13** with a conventional pincer ligand, is also an almost perfect T, but the vacancy lies *trans* to the alkenyl ligand instead of *cis*.[26]

Unlike the reaction with diphenylacetylene, the disappearance of **1**-*anti* in the presence of acetylene has been observed to be fast. Furthermore, under excess acetylene, the vinyl complex **13** has been found to be a transient reaction product rather than the final one. Due to its high solubility in hexane, **13** has been isolated pure after treating with this solvent the dry residues of reactions carried out in CH_2Cl_2. However, the yield of **13**, always poor, has been found to decrease with time due to the increasing formation of a relatively insoluble dark-colored material. This material remained soluble enough in THF for GPC analysis, which suggests that it is (or contains) polyacetylene. Two different samples, obtained after 14 and 24 h of reaction between **1** and excess acetylene (ca. 1 bar) at room temperature, have produced GPC peaks of number-average molecular weights (M_n) 2600 and 4900, respectively, with a common polydispersity ratio (M_w/M_n) of 1.19. These features suggest a living polymerization,[27] as might be expected from a structure such as that of **13**, suitable to undergo consecutive insertions (Figure 8). Despite its modest activity, complex **13** constitutes a rare example of iridium alkyne polymerization catalyst,[28] as well as a limpid illustration of the potential benefits behind the catalytic application of biPSi pincer ligands. Unfortunately, so far, similar poly- or oligomerization reactions have not been observed for other 1-alkynes.

The insertion reactions in complex **1** and their products can be further illustrated with another type of stable compounds: alkyl derivatives resulting from reactions against diazoalkanes. The reaction between **1** and the commercially available ethyl diazoacetate (EDA) has been found to afford the alkyl derivative *syn*-[IrCl{CH_2C(O)OEt}(biPSi)] (**14**). According to the generally accepted mechanism for reactions between diazoalkanes and transition metal complexes, the transformation in eq 6 likely

(26) Ghosh, R.; Zhang, X.; Achord, P.; Emge, T. J.; Krogh-Jespersen, K.; Goldman, A. S. *J. Am. Chem. Soc.* **2007**, *129*, 853–866.

(27) See, for example: Misumi, Y.; Masuda, T. *Macromolecules* **1998**, *31*, 7572–7573.

(28) (a) Lui, J.; Lam, J. W.; Tang, B. Z. *Chem. Rev.* **2009**, *109*, 5799–5867. (b) Joo, K.-S.; Kim, S. Y.; Chin, C. S. *Bull. Kor. Chem. Soc.* **1997**, *18*, 1296–1301. (c) Marigo, M.; Marsich, N.; Farnetti, E. *J. Mol. Catal. A: Chem.* **2003**, *206*, 319–329. (d) Zhang, Y.; Wang, D.; Wurst, K.; Buchmeiser, M. R. *J. Organomet. Chem.* **2005**, *690*, 5728–5735.

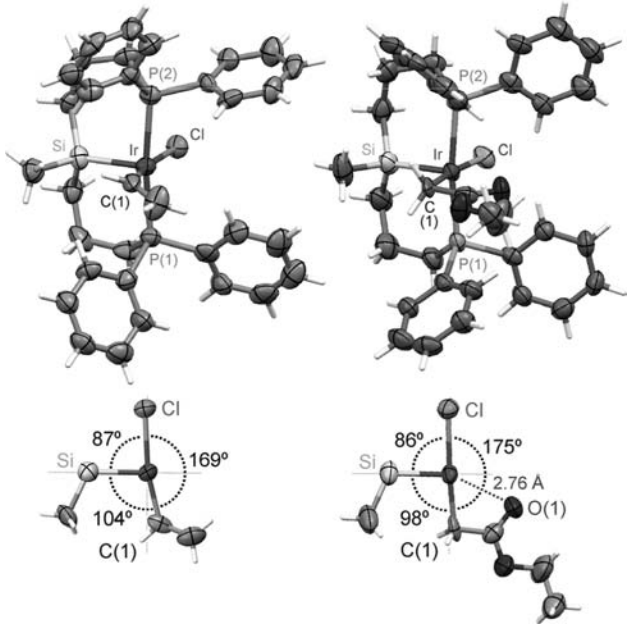

Figure 8. X-ray structures of complexes **13** and **14** and details of their equatorial planes.

proceeds via a hydride−carbene intermediate,[29] which would undergo α-insertion to form **14**. Again, the insertion reaction seems to be exclusive of *syn* isomers since, together with traces of diethyl fumarate and maleate, compound **14** is the only detectable reaction product. The reaction has been observed to complete in about 20 min at room temperature.

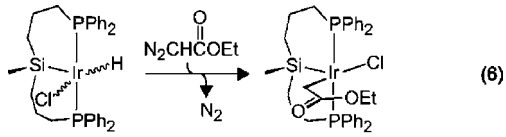

1 **14** **(6)**

The structure of **14** determined by X-ray diffraction is shown in Figure 8. Although the orientation of the ester substituent may suggest that an oxygen atom occupies the sixth coordination position, the observed Ir−O distance is again too long for a bond. Once again, the structure reveals the capability of the biPSi ligand to control the position of the coordination vacancy, in this example in the presence of an alkyl ligand.

Isomerization *anti*↔*syn*. All reactions in the previous section illustrate kinetic resolutions of equilibrium mixtures of isomers **1** due to the preferred (or exclusive) insertion into **1**-*syn*. All insertions seem to be relatively fast, but the time required for quantitative disappearance of the nonreactive **1**-*anti* strongly depends on the nature of the insertion reagent. Thus, it takes just several minutes for reaction with acetylene or EDA at room temperature but weeks in the presence of diphenylacetylene. This seems to indicate that the *anti*↔*syn* equilibration rate depends to a large extent on the presence of additives and their nature. As reference value, the pseudo-first-order rate constant for the disappearance of **1**-*anti* in the presence of diphenylacetylene has been estimated by ^{31}P NMR at 363 K as 4.32×10^{-6} s^{-1}. This value has been found independent of the diphenylacetylene concentration and therefore corresponds to a true first-order constant. This small rate constant seems compatible with the very slow isomerizations observed for the five-coordinate complexes **1**−**3** or their acetonitrile adducts **8**−**10**. In contrast, the carbonyl compounds **4**, **6**, and **7** isomerize much faster, needing just several hours to reach equilibrium distributions.

(29) (a) Cohen, R.; Rybtchinski, B.; Gandelman, M.; Rozenberg, H.; Martín, J. M. L.; Milstein, D. *J. Am. Chem. Soc.* **2003**, *125*, 6532–6546. (b) Doyle, M. P.; McKervey, M. A.; Ye, T. *Modern Catalytic Methods for Organic Synthesis with Diazo Compounds*; Wiley: New York, 1998.

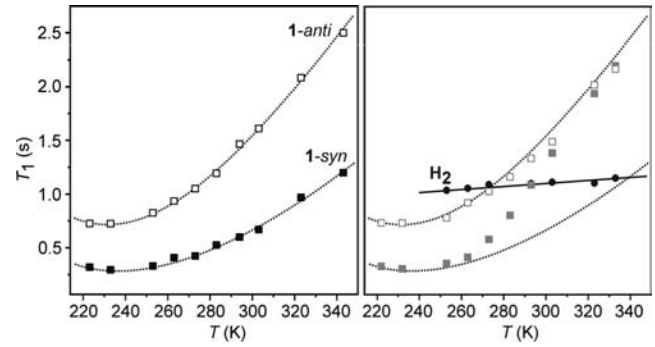

Figure 9. Evolution with temperature of the T_1 relaxation times corresponding to the ^{1}H NMR hydride signals of isomers **1** in toluene-d_8 (300 MHz): (left) in the absence and (right) in the presence of dissolved H_2.

An extreme case of fast *anti*↔*syn* exchange has been observed in the presence of dihydrogen, a reagent that does not form any detectable new product with **1**−**3** but renders isomerization rates of the same order than as NMR time scale. The fast *anti*↔*syn* exchange can be visualized with the help of Figure 9, which represents the evolution with temperature of the T_1 relaxation times corresponding to the ^{1}H NMR hydride signals of isomers **1**. Even though the exchange does not become fast enough to average or broaden the hydride NMR signals, it provokes an average of their relaxation times above 260 K. Interestingly, the T_1 values corresponding to the ^{1}H NMR signal of dissolved H_2 do not average with those of the hydrides, suggesting the lack of Ir−H/H_2 atom exchange during the *anti*↔*syn* isomerization. The same conclusion can be derived from the use of D_2 instead of H_2 since, despite the fast exchange, incorporation of deuterium into the hydride position of isomers **1** is significant only after at least 1 h of reaction. The progress of such slow H/D substitution can be conveniently followed by ^{31}P{^{1}H} NMR, since it causes observable isotopic shifts. The values of $\Delta\delta = +0.12$ and $+0.16$ ppm found for the *anti* and *syn* isomers of **1**, respectively, are of the same sign and magnitude as those previously observed in related Ir(III) complexes.[22]

A quantitative determination of *anti*↔*syn* isomerization rate constants has been carried out on solutions of the bromide complex **2** in toluene-d_8 at different dihydrogen pressures and temperatures, using spin saturation transfer methods on the ^{1}H NMR hydride signals. All kinetic information is summarized in Figure 10, which concludes that the isomerization rate depends directly on the H_2 pressure and estimates the activation parameters as $\Delta H^{\ddagger} = 7.4(\pm1)$ kcal mol^{-1} and $\Delta S^{\ddagger} = -22(\pm2)$ cal K^{-1} mol^{-1} (see Experimental Section and Supporting Information for details). The large negative enthalpy increment agrees with a second-order reaction and suggests that, despite the absence of observable intermediates, this *anti*↔*syn* isomerization begins with the coordination of dihydrogen to the five-coordinate complex. Accordingly, the fast isomerization could be related to the formation of polyhydride intermediates, the

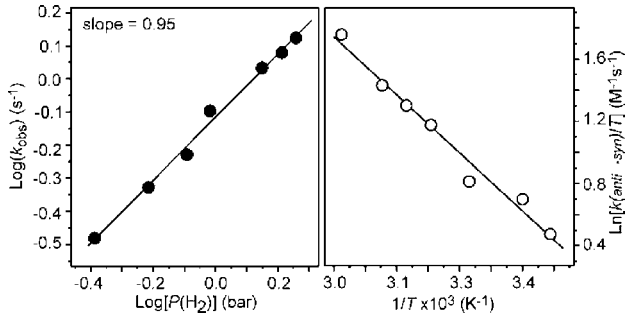

Figure 10. (Left) Dependence upon H_2 partial pressure of the pseudo-first-order rate constants (k_{obs}) for exchange between **2**-*anti* and **2**-*syn* isomers. (Right) Eyring representation of the isomerization first-order rate constants ($k(anti \rightarrow syn) = k_{obs}/[H_2]$).

behavior of which is often fluxional.[30] Nevertheless, this proposal should be qualified to account for the absence of exchange between hydrides and dihydrogen.

A possible mechanism for this *anti*↔*syn* isomerization, initiated by coordination of dihydrogen to **2** and compatible with all experimental observations, is detailed in Figure 11. Its feasibility is supported by MP2 calculations on the model of complex **2** without phenyl rings. Under such a mechanism, the isomerization takes place when the hydride ligand passes from one face of the complex to the other through the plane defined by the *mer*-coordinated biPSi ligand. The TS associated with this step resembles a σ-M-(η^2-SiH)-coordinated silane (agostic)[31] or a hypervalent Si···H—M interaction.[19] This type of TSs and intermediates has previously been observed or proposed for the isomerization of other hydride silyl complexes.[32] A similar mechanism has also previously been analyzed for compounds analogous to **1**−**3** with PCP pincer ligands, although it was found ineffective in that case.[33]

The mechanistic proposal of Figure 11 involves a *syn* adduct coordinating dihydrogen *trans* to silicon and its *anti** isomer (H_2 *trans* to hydride), those experimentally observed for other weakly coordinating ligands such as acetonitrile. Also according to the experimental evidence, the isomerization mechanism does not necessarily imply an exchange of H atoms between hydride and dihydrogen ligands. Nevertheless, such an exchange can occur in the trihydride intermediate **2**-*syn*$(H)_2$ through the high-energy TS shown in Figure 11 above the isomerization coordinate. Although the calculations have been limited to a simple model of complex **2** and are not intended to accurately reproduce experimental energies, the low overall isomerization barrier seems compatible with the experimental activation enthalpy (10.1 vs 7.4 ± 1 kcal mol^{-1}).

The calculated mechanism does not include a TS for dihydrogen coordination to **2**-*syn* because it could not be located. As discussed in previous sections, on the basis of experimental data, given the structure of the complex, the activation energy for ligand coordination *trans* to silicon is expected to be very low, especially for a small incoming ligand such as dihydrogen in a model complex without phenyl rings. A similar circumstance has been experimentally observed for other d^6 complexes of T structure, whose reaction kinetics with dihydrogen depend only on the rates of reactant diffusion in solution.[34] By contrast, the model of **2**-*anti* needs to invest 5.8 kcal mol^{-1} to reorganize its equatorial plane for dihydrogen coordination *trans* to hydride. Interestingly, the experiments described previously have shown that a similar reorganization of **1**-*anti* to coordinate acetonitrile requires an activation enthalpy of 11.4(±1.1) kcal mol^{-1}, higher than that of the entire isomerization process in the presence of H_2. This suggests that the mere coordination of dihydrogen to **2**-*anti* should not be discarded as potential rate-determining step of the whole *anti*↔*syn* isomerization process. In fact, this possibility would perfectly fit with the negligible kinetic isotope effects (KIEs) (very close to 1) that have been observed for isomerizations using either the deuteride isotopomer of **2** or D_2 instead of H_2. With regard to the literature data, the elementary steps of H_2 coordination to unsaturated complexes typically display KIE values (k_H/k_D) very close to 1[34a,35] but equilibrium isotope effects (EIE = K_H/K_D) significantly lower than this value.[36] Due to the latter, any rate-limiting step beyond the reversible H_2 coordination should lead to a significant inverse KIE, reflecting such an EIE.

The mechanism of Figure 11 involves some Ir(V) intermediates. This oxidation state is emerging as relatively common in stable complexes with ligands such as hydride, silyl, alkyl, and boryl and is increasingly considered a likely alternative in the context of mechanistic discussion.[37] Assuming the key TS of the mechanism to be an agostic Ir(III) species, the acceleration of the *anti*↔*syn* isomerization under H_2 can be attributed to the ability of this reactant to provoke the oxidation state Ir(V), from which the formal reductive elimination leading to the agostic TS should be favored. Accordingly, acetylene, another potential oxidative addition reagent, has also been observed to catalyze this isomerization prior to insertion. A calculated

(30) (a) Loza, M.; Faller, J. W.; Crabtree, R. H. *Inorg. Chem.* **1995**, *34*, 2937–294. See also: (b) Kubas, G. J. *Metal Dihydrogen and σ-Bond Complexes*; Kluwer Academic/Plenum, New York, 2001. (c) Kubas, G. J. *Comprehensive Organometallic Chemistry*, 3rd ed.; Mingos, D. M. P., Crabtree, R. H., Eds.; Elsevier: Amsterdam, 2007; Vol. 1, pp 671−698. (d) Morris, J. H.; Jessop, P. G. *Coord. Chem. Rev.* **1992**, *121*, 155–289. (e) Heinekey, D. M.; Oldham, W. J., Jr. *Chem. Rev.* **1993**, *93*, 913–926.

(31) (a) Delpech, F.; Sabo-Etienne, S.; Daran, J.-C.; Chaudret, B.; Hussein, K.; Marsden, C. J.; Barthelat, J.-C. *J. Am. Chem. Soc.* **1999**, *121*, 6668–6682. (b) Perutz, R. N.; Sabo-Etienne, S. *Angew. Chem., Int. Ed.* **2007**, *46*, 2578–2592. Stable M(η^2-Si-H) agostic species have been isolated for Ru(II), Ni(II), and Pd(0): (c) Montiel-Palma, V.; Muñoz-Hernández, M. A.; Ayed, T.; Barthelat, J.-C.; Grellier, M.; Vendier, L.; Sabo-Etienne, S. *Chem. Commun.* **2007**, 3963–3965. (d) Chen, W.; Shimada, S.; Tanaka, M.; Kobayashi, Y.; Saigo, K. *J. Am. Chem. Soc.* **2004**, *126*, 8072–8073. (e) Takaya, J.; Nobuharu, I. *Organometallics* **2009**, *28*, 6636–6638.

(32) (a) Ampt, K. A. M.; Duckett, S. B.; Perutz, R. N. *Dalton Trans.* **2004**, 3331–3337. See also: (b) Câmpian, M. V.; Clot, E.; Eisenstein, O.; Helmstedt, U.; Jasim, N.; Perutz, R. N.; Whitwood, A. C.; Williamson, D. *J. Am. Chem. Soc.* **2008**, *130*, 4375–4385.

(33) Li, S.; Hall, M. B. *Organometallics* **1999**, *18*, 5682–5687.

(34) (a) Bakhmutov, V. I.; Bertrán, J.; Esteruelas, M. A.; Lledós, A.; Maseras, F.; Modrego, J.; Oro, L. A.; Sola, E. *Chem. Eur. J.* **1996**, *2*, 815–825. See also: (b) Zhang, K.; González, A. A.; Hoff, C. D. *J. Am. Chem. Soc.* **1989**, *111*, 3627–3632. (c) Hall, C.; Jones, W. D.; Mawby, R. J.; Osman, R.; Perutz, R. N.; Whittlesey, M. K. *J. Am. Chem. Soc.* **1992**, *114*, 7425–7435.

(35) Janak, K. E. In *Comprehensive Organometallic Chemistry*, 3rd ed.; Mingos, D. M. P., Crabtree, R. H., Eds.; Elsevier: Amsterdam, 2007; Vol. 1, p 561.

(36) (a) Gusev, D. G.; Bakhmutov, V. I.; Grushin, V. V.; Vol'pin, M. E. *Inorg. Chim. Acta* **1990**, *177*, 115–120. (b) Hauger, B. E.; Gusev, D. G.; Caulton, K. G. *J. Am. Chem. Soc.* **1994**, *116*, 208–214. (c) Kubas, G. J. *Chem. Rev.* **2007**, *107*, 4152–4205.

(37) See for example: (a) Mann, B. E.; Masters, C.; Shaw, B. L. *J. Inorg. Nucl. Chem.* **1971**, *33*, 2195–2204. (b) Fernandez, M. J.; Maitlis, P. M. *Organometallics* **1983**, *2*, 164–165. (c) Gutiérrez-Puebla, E.; Monge, A.; Nicasio, M. C.; Pérez, P. J.; Poveda, M. L.; Carmona, E. *Chem. Eur. J.* **1998**, *4*, 2225–2236. (d) Alaimo, P. J.; Bergman, R. G. *Organometallics* **1999**, *18*, 2707–2717. (e) Klei, S. R.; Tilley, T. D.; Bergman, R. G. *J. Am. Chem. Soc.* **2000**, *122*, 1816–1817. (f) Kawamura, K.; Hartwig, J. F. *J. Am. Chem. Soc.* **2001**, *123*, 8422–8423.

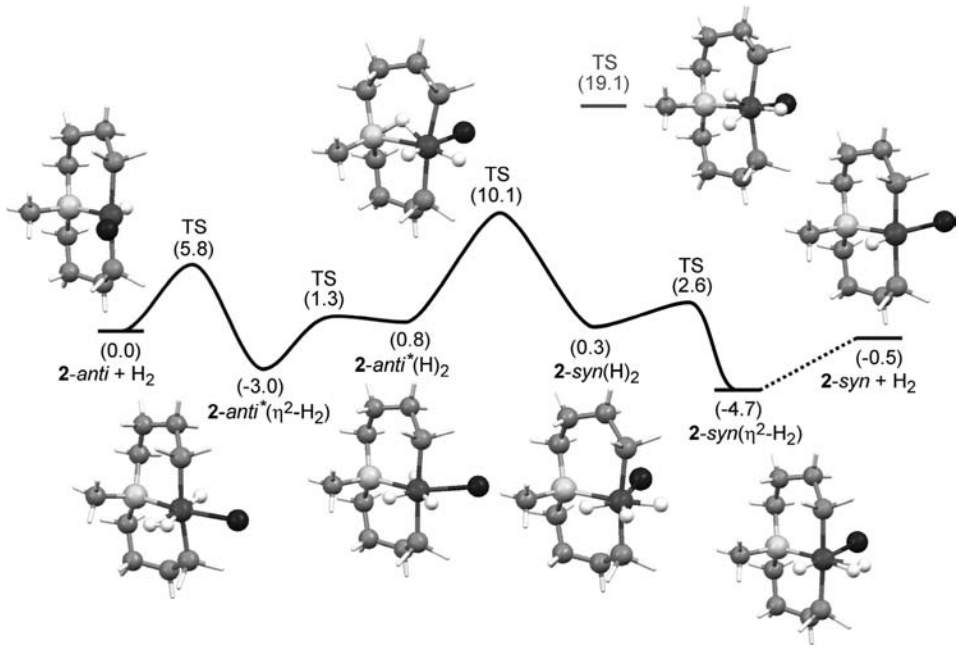

Figure 11. Mechanism for the *anti*↔*syn* isomerization under H_2 based on MP2-calculated structures and energies (kcal mol^{-1}, without corrections). Most transition states have been omitted for clarity.

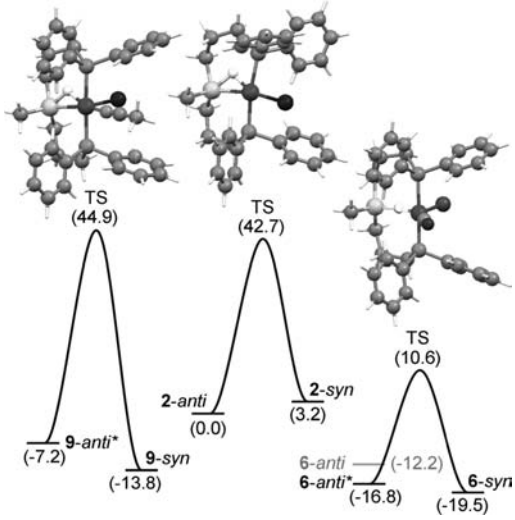

Figure 12. Calculated energies (kcal mol^{-1}, without corrections) and optimized transition states for the *anti*↔*syn* isomerization of complex **2** (center) and its carbonyl (right) and acetonitrile (left) adducts **6** and **9**, respectively.

reaction coordinate showing the intermediates and TSs of the *anti*↔*syn* isomerization in the presence of acetylene and its subsequent insertion has been included as Supporting Information. An agostic TS analogous to that in Figure 11 has been located just 4.3 kcal mol^{-1} above **2**-*anti*.

The deduced mechanism of isomerization could be extrapolated to the absence of oxidative addition reagents if the key agostic TSs could be generated through formal reductive eliminations in Ir(III) species. This possibility has been explored by calculation, in this case using the complete model of complex **2** (including phenyls by UFF methods in ONIOM approach). The TS for a direct isomerization of the five-coordinate species has been found 42.7 kcal mol^{-1} above **2**-*anti* (Figure 12). Interestingly, the calculated isomerization barrier further increases in the acetonitrile adduct **9** but decreases to 30.1 kcal mol^{-1} in the six-coordinate carbonyl compound **6**. These barriers are in good qualitative agreement with the expected electronic effect of each ligand on the energy of an Ir(I) TS and even seem to correlate with structural parameters such as the Ir−Si bond distances (Supporting Information). Even though the quantitative aspects of this mechanism remain susceptible to further elaboration, so far it is entirely consistent with the experimental observations on the system. Moreover, the mechanism provides a rationale for the previously reported counterintuitive observation of five-coordinate Ru(II) hydride complexes that are rigid in solution but form rapidly isomerizing octahedral CO adducts.[38]

Conclusions

The studies described herein offer a detailed description of the behavior of the biPSi ligand (κ-*P,P,Si*-Si(Me){$(CH_2)_3PPh_2$}$_2$) in the coordination sphere of the five-coordinate iridium(III) complexes [IrXH(biPSi)], together with representative examples of their coordination adducts and insertion products.

This type of diphosphine can be considered a particular class of pincer ligand due to its capability of forcing *cis* relative positions between the vacant sites of unsaturated complexes and reactive ligands such as hydride, alkyl, and alkenyl. Nevertheless, an effective use of such vacant sites for coordination and subsequent reactions requires the connivance of steric factors. Both the success of this strategy toward more reactive unsaturated metal complexes and its limitations have a common origin in the large *trans* influence of the sp^3 silyl moiety, which overcomes that of other ligands to dictate the ground-state geometry around the metal, although at the expense of diminishing the binding energies of incoming ligands below contributions that are otherwise secondary. As a consequence of the latter, the coordination behavior of these complexes, and hence their reactivity thereafter, becomes especially sensitive to details of the ligand environment. As an example, changing the halide

(38) Zhou, X.; Stobart, S. R. *Organometallics* **2001**, *20*, 1898–1900.

ligand of [IrXH(biPSi)] from chloride to iodide switches the stable coordination position of CO from *cis* to hydride to *trans*.

In the particular case of the [IrXH(biPSi)] complexes, such a sensitivity to the ligand environment results in more reactive *syn* isomers. Actually, all reagents studied in the course of this work have been found able to discriminate to some extent between *anti* and *syn* isomers, in some cases resolving the isomeric mixtures by selective reaction with the *syn* compound. First, this has minimized the consequences of dealing with mixtures of isomers instead of pure compounds—another inevitable outcome of the sp^3 silyl group, especially undesirable if the objective is a single-site homogeneous catalyst. In addition, the effectiveness of certain reagents in the kinetic resolution of isomers has led to the recognition of an *anti*↔*syn* isomerization mechanism via M-(η^2-SiH) agostic TSs. In agreement with such a mechanism, the isomerization is accelerated by potential ligands that stabilize the oxidation state Ir(I), but it can also be catalyzed by oxidative addition reagents providing access to Ir(V) intermediates.

It turns out from this study that PSiP pincer ligands control the position of coordination vacancies, produce resolvable mixtures of isomeric hydrides, and provoke coordination properties that are especially sensitive to the ligand environment. The design of complexes, ligands, and reaction conditions that can turn such exceptional features into advantages and/or new catalytic applications is a challenge, for which we expect the experimental observations and conclusions of this work to be a guide.

Experimental Section

General Methods. All manipulations were carried out under argon by standard Schlenk techniques or in an argon-filled MBraun drybox. Solvents were obtained from a solvent purification system (Innovative Technologies). Deuterated solvents were dried with appropriate drying agents and degassed with argon prior to use. C, H, and N analyses were carried out in a Perkin-Elmer 2400 CHNS/O analyzer. MALDI-TOF mass spectra were obtained on a Bruker Microflex mass spectrometer using 1,8,9-trihydroxyanthracene as matrix. Infrared spectra were recorded in KBr using a Perkin-Elmer Spectrum One FT-IR spectrometer. NMR spectra were recorded on Bruker Avance 400 and 300 MHz spectrometers. ^{1}H (400.13 or 300.13 MHz) and ^{13}C (100.6 or 75.5 MHz) NMR chemical shifts were measured relative to partially deuterated solvent peaks but are reported in ppm relative to TMS. ^{31}P (162.0 or 121.5 MHz) and ^{29}Si (59.6 or 79.5 MHz) chemical shifts were measured relative to H_3PO_4 (85%) and TMS, respectively. In general, NMR spectral assignments were achieved through ^{1}H COSY, ^{1}H NOESY, ^{13}C APT, and ^{1}H/^{13}C HSQC experiments. The molecular weights (M_n and M_w) and polydispersity indices (M_w/M_n) of the polyacetylene samples were measured by GPC with a Waters 2695 autosampler chromatograph equipped with Phenogel linear mixed columns and a Waters 2487 dual-lambda UV detector, which was previously calibrated with polystyrene standards (molecular weight limit up to 1×10^7). The samples were eluted at 35 °C with THF at a flow rate of 1 mL min^{-1}. The starting complex [Ir(μ-Cl)(COD)]$_2$[39] and the diphosphine bis(3-diphenylphosphinopropyl)methylsilane (biPSiH)[40] were prepared by known procedures. All other reagents were commercially available and were used as received. Experimental details and spectroscopic characterizations of the new complexes are presented in the Supporting Information.

NMR Equilibrium and Kinetic Studies. The NMR sample temperature was calibrated using the temperature dependence of the chemical shifts of MeOH and ethylene glycol. Errors in the magnitudes obtained from Van't Hoff or Eyring regressions were estimated through conventional error propagation formulas,[41] assuming 1 K error in the temperature and a 10% error in the constant. All numerical data obtained in these studies are presented in the Supporting Information.

The coordination of $CDCl_3$ or CD_2Cl_2 to the *syn* isomers of **1**−**3** was studied using the ^{31}P{^{1}H} NMR chemical shifts because their variation with temperature was greater than that of other chemical shifts. The equilibrium constants (K) for solvent (sol) coordination to the five-coordinate complex (5C) are defined in the sense of formation of the six-coordinate adduct (6C) and can also be expressed in terms of the molar fraction (x) of the 5C species:

$$K = [6C]/[5C][sol] = (1 - x)/(x[sol])$$

For a fast equilibrium on the NMR time scale, the chemical shift of the signal due to an average of the 5C and 6C species is also a function of the molar fraction and therefore can also be expressed in terms of the equilibrium constant:

$$\delta = \delta(6C) + \{\delta(5C) - \delta(6C)\}x$$

$$\delta = \delta(6C) + \{\delta(5C) - \delta(6C)\}\{1/(1 + K[sol])\}$$

Writing K as a function of $\Delta H°$ and $\Delta S°$ ($\ln K = -\Delta H°/RT + \Delta S°/R$) and operating, the dependence of δ upon the inverse of temperature takes the form typical of a sigmoidal function:

$$\delta = \delta(6C) + \{\delta(5C) - \delta(6C)\}/[1 + \exp\{(1/T) - (R \ln[sol] + \Delta S°)/\Delta H°\}/(-R/\Delta H°)\}]$$

$$y = A2 + (A1 - A2)/[1 + \exp\{(x - x_0)/dx\}]$$

The experimental values of δ vs $1/T$ can then be adjusted to sigmoidal functions to give the equilibrium enthalpy and entropy increments. Since the samples were rather diluted (ca. 10 mg in 0.5 mL), the solvent concentration was directly estimated from its density: 15.24 M (1.32 g cm^{-3}) for CD_2Cl_2 and 12.29 M (1.48 g cm^{-3}) for $CDCl_3$. In this case, the errors in $\Delta H°$ and $\Delta S°$ were directly propagated from the assumed errors in temperature and δ: 1 K and 0.1 ppm, respectively.

The stability of the acetonitrile adducts was studied in toluene-d_8 samples containing known concentrations of the metal complex (around 0.02 M) and acetonitrile (in the range 2−4 μL). The samples used to study *anti** isomers were prepared immediately before use, whereas those dedicated to the *syn* isomers were allowed to evolve for several weeks until complete transformation into these isomers. The equilibrium constants for the formation of **9**−**11**-*syn* were obtained from the ^{31}P{^{1}H} NMR spectra of fast equilibria (above 313 K), using the same equations detailed in the previous case with [sol] = [NCMe]. Since, at room temperature, the equilibria are well displaced toward the 6C species, their chemical shifts, δ(6C), were taken from these spectra, while δ(5C) were obtained from samples of the pure 5C precursors. Equilibrium ratios [6C]/[5C] at various temperatures were then obtained from the averaged chemical shifts, and the actual acetonitrile concentrations were calculated from the initial ones and the position of each equilibrium. The equilibrium constants involving *anti** isomers were obtained from slow equilibria at low temperature. The [6C]/[5C] ratios were obtained by integration of their corresponding ^{1}H NMR hydride signals. The acetonitrile concentrations could not be estimated by integration due to the overlap of various signals. In turn, [NCMe] values were calculated from the known initial concentrations, taking into account that, in part, it is coordinated to both *anti** and *syn* isomers.

(39) Usón, R.; Oro, L. A.; Cabeza, J. A. *Inorg. Synth.* **1985**, *23*, 126–130.
(40) Stobart, S. R.; Joslin, F. L. *Inorg. Chem.* **1993**, *32*, 2221–2223.
(41) (a) Taylor, J. R. *An Introduction to Error Analysis*, 2nd ed.; University Science Books: Mill Valley, CA, 1982. (b) Morse, P. M.; Spencer, M. O.; Wilson, S. R.; Girolami, G. S. *Organometallics* **1994**, *13*, 1646–1655.

First-order rate constants for acetonitrile dissociation from **8**-*anti** were determined by spin saturation transfer, following the Forsén−Hoffman method.[42] The presaturation pulse was applied on the ^{1}H NMR signal corresponding to the hydride ligand of **1**-*anti*, and its effect was measured in the intensity of the **8**-*anti** hydride signal.

Determination of the **1**-*anti*↔**1**-*syn* isomerization rate constant in the presence of diphenylacetylene was carried out by ^{31}P{^{1}H} NMR monitoring of 0.04 M solutions of **1** at 363 K. Two samples of alkyne concentrations 0.4 and 1 M, respectively, gave coincident results.

Determinations of the *anti*↔*syn* isomerization rate constants in presence of H_2 were carried out in PTFE-valved sealable 5 mm NMR tubes (Wilmad). Each tube, previously filled with an aliquot of a common solution of **2** in toluene-d_8 ([**2**] ca. 0.02 M), was simultaneously connected to a Schlenk manifold, to allow for reaction manipulation and degassing, and to a high-pressure H_2 source. This latter connection was made through an electronic pressure meter/controller (El-Press, Bronkhorst HI-TEC) that allowed us to select the operating pressure in the range 0−4 bar (absolute pressure) from a computer, thereby also allowing us to measure the resulting pressure once the system reached equilibrium. The freeze−thawed samples of **2** were loaded with H_2 at the desired pressure, allowed to equilibrate at room temperature for 30 min, and sealed. The partial pressure of H_2 was calculated from the pressure measured at this point and the vapor pressure of toluene.[43] In experiments above room temperature, the pressure that developed inside the NMR tube was calculated assuming ideal gas behavior. The values of H_2 solubility at different partial pressures and temperatures were obtained from literature data[44] and the application of Henry's law. T_1 relaxation times were measured by the inversion−recovery method. The pseudo-first-order rate constants (k_{obs}) were obtained by spin saturation transfer, applying the saturating pulse on the hydride signal of the minor isomer **2**-*syn* and measuring the intensity change of the hydride signal of **2**-*anti*.

X-ray Crystallography. X-ray data were collected at 100.0(2) K on a Bruker SMART APEX CCD with graphite-monochromated Mo Kα radiation (λ = 0.71073 Å). Data were collected over the complete sphere by a combination of four sets. Data were corrected for absorption by using a multiscan method applied with the SADABS program.[45] The structures were solved by the Patterson method and refined by full-matrix least-squares on F^2 using Bruker SHELXTL program package,[46] including isotropic and subsequently anisotropic displacement parameters. Weighted R factors (R_w) and goodness of fit (S) are based on F^2, and conventional R factors are based on F. Hydride ligands were located, but not all of them refined appropriately. In such cases the Ir−H distance was fixed to 1.59(1) Å (average value found in the Cambridge Structural Database). The rest of the hydrogen atoms were calculated using a restricted riding model on their respective carbon atoms with the thermal parameter related to the bonded atom. All the highest electronic residuals were observed in close proximity of the Ir centers and make no chemical sense. Crystallographic data are summarized in the Supporting Information.

Computational Details. Calculations were executed using the Gaussian suite of programs[47] and ONIOM-type approaches. The low-level calculations were MP2. The inner electrons of Ir, Br, Si, and P atoms were described using the effective core potential LANL2DZ.[48] The outer electrons were described with a double-ζ basis set,[49] plus p polarization functions for the hydrides, d for C, P, Si, and Br atoms,[50] and diffuse d[51] and f[52] polarization shells for Ir. The second layer consisted of a QCISD(T) approach for Ir and the atoms coordinated to it: Br, Si, P, hydrides, and acetylene C atoms. In calculations including phenyl groups, the third layer used a molecular mechanics force field (UFF) to estimate their steric effects.

The characterization of each structure as either minimum or TS used harmonic vibrational frequency calculations on an early level of calculation, i.e., at the MP2 level not including polarization functions for most atoms [ONIOM MP2/LANL2DZ+(f,d,p):HF/LANL1DZ] or at the DFT level[53] by using the B3LYP functional[54] [B3LYP/LANL2DZ+(f,d,p)]. After this characterization, the structures and energies were reoptimized at the levels MP2/LANL2DZ+(f,d,p) and ONIOM QCISD(T)/LANL2DZ+(f,d,p):MP2/LANL2DZ+(f,d,p), respectively. For models with phenyl rings, the final levels of calculation were ONIOM MP2/LANL2DZ+(f,d,p):UFF for the structures and ONIOM QCISD(T)/LANL2DZ+(f,d,p):MP2/LANL2DZ+(f,d,p):UFF for the energy.

Acknowledgment. We thank Stephen R. Stobart for his valuable contributions to this work. This research was supported by the Spanish MICINN (grants CTQ2006-01629, CTQ2009-08023, and Consolider Ingenio 2010 INTECAT CSD2006-0003).

Supporting Information Available: Synthesis and characterization details, tables of bond distances and angles, crystal data, figures and tables on the thermodynamic and kinetic determinations, complete ref 47, a calculated reaction coordinate for the *anti*↔*syn* isomerization/insertion sequence in presence of acetylene; information (Cartesian coordinates, absolute energies) on the calculated structures; and X-ray crystallographic file for the complexes **2**-*anti*, **2**-*syn*, **3**-*syn*, **6**-*syn*, **8**-*syn*, **11**-*anti*, **13**, and **14** in CIF format. This material is available free of charge via the Internet at http://pubs.acs.org.

JA102479H

(42) (a) Faller, J. W. In *Determination of Organic Structures by Physical Methods*; Nachod, F. C., Zuckerman, J. J., Eds.; Academic Press: New York and London, 1973. (b) Sanders, J. K. M.; Hunter, B. K. *Modern NMR Spectroscopy, A Guide for Chemists*, 2nd ed.; Oxford University Press: Oxford, 1993.
(43) *TRC Thermodynamic Tables: Hydrocarbons*; National Institute of Standards and Technology: Boulder, CO; Vol. VIII, p Kb3290, 1995.
(44) Cook, M. W.; Hanson, D. N.; Adler, B. J. *J. Chem. Phys.* **1957**, *26*, 748–751.
(45) Blessing, R. H. *Acta Crystallogr.* **1995**, *A51*, 33–38. *SADABS: Area-detector absorption correction*; Bruker-AXS: Madison, WI, 1996.
(46) *SHELXTL*, v. 6.10; Bruker-AXS: Madison, WI, 2000. Sheldrick, G. M. *SHELXS-86 and SHELXL-97*; University of Göttingen: Göttingen, Germany, 1997.
(47) Frisch, M. J.; et al.; *Gaussian 03*, Revision C.02; Gaussian, Inc.: Wallingford, CT, 2004.
(48) Hay, P. J.; Wadt, W. R. *J. Chem. Phys.* **1985**, *82*, 299–310.
(49) (a) Huzinaga, S. *J. Chem. Phys.* **1965**, *42*, 1293–1302. (b) Dunning, T. H. *J. Chem. Phys.* **1970**, *53*, 2823–2833.
(50) Höllwarth, A.; Böhme, S.; Dapprich, S.; Ehlers, A. W.; Gobbi, A.; Jonas, V.; Köhler, K. F.; Stegmann, R.; Veldkamp, A.; Frenking, G. *Chem. Phys. Lett.* **1993**, *208*, 237–240.
(51) Couty, M.; Hall, M. B. *J. Comput. Chem.* **1996**, *17*, 1359–1370.
(52) Ehlers, A. W.; Böhme, S.; Dapprich, S.; Gobbi, A.; Höllwarth, A.; Jonas, V.; Köhler, K. F.; Stegmann, R.; Veldkamp, A.; Frenking, G. *Chem. Phys. Lett.* **1993**, *208*, 111–114.
(53) (a) Parr, R. G.; Yang, W. *Density Functional Theory of Atoms and Molecules*; Oxford University Press: Oxford, U.K., 1989. (b) Ziegler, T. *Chem. Rev.* **1991**, *91*, 651–667.
(54) (a) Lee, C.; Yang, W.; Parr, R. G. *Phys. Rev. B* **1988**, *37*, 785–789. (b) Becke, A. D. *J. Chem. Phys.* **1993**, *98*, 5648–5652. (c) Stephens, P. J.; Devlin, F. J.; Chabalowski, C. F.; Frisch, M. J. *J. Phys. Chem.* **1994**, *98*, 11623–11627.